NJC

PAPER

Cite this: *New J. Chem.*, 2016, 40, 1175

Green-emitting fluorescence Ag clusters: facile synthesis and sensors for Hg^{2+} detection†

Chang Zhang,*[ab] Zhi Guo,[ab] Guiqiu Chen,*[ab] Guangming Zeng,[ab] Ming Yan,[ab] Qiuya Niu,[ab] Lingzhi Liu,[ab] Yanan Zuo,[ab] Zhenzhen Huang[ab] and Qiong Tan[ab]

Received (in Montpellier, France) 26th August 2015,
Accepted 5th November 2015

DOI: 10.1039/c5nj02268a

www.rsc.org/njc

Bovine serum albumin (BSA) has proven to be particularly effective for the synthesis of Ag clusters due to its free cysteine residue in an alkaline environment. However, the currently used BSA-directed synthesis method is still complicated and uses BSA only as a stabilizing agent. In this study, we developed a simpler method for the synthesis of new fluorescent Ag clusters using BSA as a reducing and stabilizing agent. The as-prepared Ag clusters exhibited high green fluorescence emission (~548 nm). Different changes in the pH were used for the synthesis of Ag clusters with different sizes. The results indicated that higher pH led to a smaller size. Furthermore, the Ag clusters were successfully applied in Hg^{2+} detection. The lowest detectable concentration was estimated to be 4.0 nM with a large range from 4.0 nM to 400.0 nM. MTT assays showed that the biotoxicity of the as-prepared Ag clusters was significantly lower than that of $NaBH_4$-reduced nano-silver.

1. Introduction

Metal clusters, which contain metal nanoparticles smaller than 2 nm, are collections of two to several hundred metal atoms.[1,2] Such nanoclusters have received increasing attention in recent years due to their unique size- and shape-dependent catalytic, optical, electrical, magnetic, and chemical properties.[3–12] Of the various metal clusters reported to date, Ag-based clusters are of special interest as promising probes due to their ultra-small size, low toxicity, and high fluorescence.[3,13,14] These clusters have a discrete electronic state and exhibit strong size-dependent fluorescence at room temperature.[15]

The synthesis of Ag nanoclusters in aqueous solutions, however, is difficult because Ag nanoclusters tend to aggregate. Recently, many methods for the synthesis of water-soluble Ag clusters have been developed. Cathcart *et al.*[16] reported a novel approach that involved a cyclic reduction under oxidative conditions to prepare a single dominant species of chiral thiol-stabilized silver nanoclusters. Adhikari and Banerjee developed a single-step facile synthesis of highly emissive, water-soluble, fluorescent Ag nanoclusters using a small molecule, dihydrolipoic acid.[17] Xu *et al.*[18] successfully synthesized highly fluorescent, stable, water-soluble Ag nanoclusters through a convenient sonochemical approach using a simple polyelectrolyte, polymethylacrylic acid, as a capping agent. Moreover, synthetic methods for the preparation of Ag clusters using various templated assemblies, such as DNA,[19–23] polypeptides,[24,25] and proteins,[26–28] have been documented.

The clusters obtained using these approaches have generally been produced from Ag^+ and strong reducing agents, such as $NaBH_4$, and utilize an organic molecule to cap the final cluster.[2] Although these methods can yield fluorescent nanoclusters, strong reducing agents can potentially introduce side effects when the organic molecule–cluster hybrids are used in biological fields.[2,29] Moreover, there are some drawbacks in terms of the relatively low quantum yield and size control. The synthesized clusters also exhibit low biocompatibility. It is always a real challenge to produce clusters that can be more effectively used in clinical applications.

In this manuscript, we present a novel and easily controlled biomimetic synthesis of water-soluble fluorescent Ag nanoclusters in aqueous solutions using BSA as a reducing and capping agent. BSA was chosen in this study because it is widely used and commercially available and because it has been proven to work in the synthesis of fluorescent metal nanoclusters.[3,26,30–36] Different Ag clusters were formed and anchored *via* BSA *in situ*

[a] College of Environmental Science and Engineering, Hunan University, Changsha 410082, P. R. China. E-mail: zhangchang@hnu.edu.cn, gqchen@hnu.edu.cn; Fax: +86 731 88823701; Tel: +86 731 88822829
[b] Key Laboratory of Environmental Biology and Pollution Control (Hunan University), Ministry of Education, Changsha 410082, P. R. China

† Electronic supplementary information (ESI) available: The UV-vis absorption spectrum and the TEM image of the citrate-stabilized AgNPs (Fig. S1). XPS spectra of the Ag clusters (Fig. S2). Photographs of various Ag cluster solutions prepared by controlling the pH (Fig. S3). UV-vis absorption spectra of the solutions illustrating the effect of pH, XRD patterns of dried Ag cluster materials, EDS data of fluorescent AgNCs and FT-IR spectra obtained from samples (Fig. S4). Effects of pH on the fluorescence quenching of Ag clusters (Fig. S5). Additional details of the dynamic light scattering (Fig. S6) and zeta potential measurements (Fig. S7) of the BSA–Ag clusters and citrate–AgNPs used in the toxicity study. See DOI: 10.1039/c5nj02268a

under different pH conditions, and no other adventitious reducing agents were used. The effect of pH on the particle size was assessed. Moreover, the Ag nanoclusters were successfully applied in aqueous Hg^{2+} quantification. The high biocompatibility of the biomimetic clusters *versus* $NaBH_4$-reduced AgNPs was studied using the model species *Escherichia coli* (CMCC 44102). This biomimetic method opens up a new pathway for the preparation of versatile fluorescent clusters with potential applications in bioimaging, chemical sensing, and single-molecule studies.

2. Experimental section

2.1 Chemicals

All of the chemical components were of analytical grade and used as received without further purification. All of the aqueous solutions used in this study were prepared with sterilized Milli-Q water (18.25 MΩ cm, UPT-11-40, China). $AgNO_3$ was dissolved in sterilized Milli-Q water (MQ) to obtain a final concentration of 74 mmol L^{-1} for the preparation of $[Ag(S_2O_3)_2]^{3-}$. Stock solutions of 150 mmol L^{-1} $Na_2S_2O_3$ and 1.0 g L^{-1} BSA were prepared by dissolving the appropriate amounts of $Na_2S_2O_3$ and BSA in sterilized Milli-Q water, respectively.

2.2. Synthesis of Ag nanoclusters and AgNPs

According to the literature with slight modifications.[3] A detailed procedure is described as follows: several millilitres of BSA and 24 mL of the as-prepared $[Ag(S_2O_3)_2]^{3-}$ solution were added to a flask under stirring; the amount of BSA added was changed to ensure that the final concentrations were as desired. The total volume of the mixture in the flask was adjusted to 113 mL. The pH was then adjusted to alkalinity with 10 mg L^{-1} NaOH, and the effect of different pH values in the pH range of 11–13 on the synthesis was investigated. All of the samples were sealed and shaken at 150 r min^{-1} and room temperature in the dark for 48 h without disturbance. The as-synthesized mixture was filtered, and the obtained Ag clusters were stored at 4 °C for later use.

$[Ag(S_2O_3)_2]^{3-}$ was prepared by slowly dropping 83 mL of $AgNO_3$ solution into 100 mL of $Na_2S_2O_3$ solution in a 200 mL beaker under vigorous stirring with a magnetic stirrer. After 0.5 h of additional stirring at room temperature, the final solution was stored at 4 °C in the dark until further use.

2.3. Characterization of Ag nanoclusters

The UV-vis absorption and fluorescence spectra were obtained using a UV-visible spectrophotometer (Model UV-2550, Shimadzu Company, Kyoto, Japan) and a Perkin-Elmer LS-55 spectrofluorimeter (UK), respectively. The TEM measurement was made using a JEOL JEM-3010 transmission electron microscope (Beijing, China) with an accelerating voltage of 200 kV. The sample for TEM characterization was prepared by placing a drop of the sample solution on a carbon-coated copper grid and allowing it to dry at room temperature. The hydrodynamic diameters and zeta (ζ) potentials of the particles were quantified by dynamic light scattering (DLS) conducted using a Malvern Zetasizer (Nano-ZS, Malvern Instrument, U.K.). X-ray photoelectron spectroscopy (XPS) was analyzed using ESCALAB 250Xi (Thermo Fisher-VG Scientific, USA). Atomic fluorescence measurements were performed on an atomic fluorescence spectrometer (AFS-9700, Beijing, China).

2.4. Detection of Hg^{2+}

A typical Hg^{2+} detection procedure was conducted as follows. First, 20 μL of different concentrations of Hg^{2+} solution and 30 μL of 20 mM 2,6-pyridinedicarboxylic acid (PDCA) were mixed uniformly in a 500 μL volumetric pipe. Then, the as-prepared Ag clusters (120 μL) were added to the mixture solution. Finally, the fluorescence emission intensities of different concentrations of Hg^{2+} were monitored after 9 min. For the sensitivity experiment, various concentrations of Hg^{2+} (0, 4.0, 10.0, 40.0, 100.0, 400.0, 1000.0, 4000.0, 10 000.0, and 40 000.0 nM) were added, respectively. To evaluate the selectivity of Ag clusters for Hg^{2+} detection, various metal ion salts (K^+, Ca^{2+}, Mg^{2+}, Li^{2+}, Pb^{2+}, Zn^{2+}, Mn^{2+}, Ni^{2+}, Cr^{3+}, Fe^{3+}, Co^{2+}, Cu^{2+}, Cd^{2+}, Al^{3+}) of 1.0 mM were used in the selectivity experiment. The lake water and river water taken from Taozi Lake and Xiangjiang River in Changsha City were used as the real water samples for detection. Along the detection process, 0.1 M sodium phosphate buffer was used to equilibrate the reaction system.

2.5. Toxicity of Ag clusters

To compare the toxicity of the Ag clusters, the inhibition ratio of the Ag clusters and the citrate-stabilized AgNPs toward *Escherichia coli* was studied. All of the selected AgNPs and Ag clusters were of similar size (Fig. S5, ESI†) and exhibited a similar zeta (ζ) (Fig. S6, ESI†) potential. The AgNPs and Ag clusters were washed and filtered continuously until the Ag^+ concentration in the filtrate was below the detection limit of flame atomic absorption spectrometry (markedly below the minimum added level of 0.3 μg mL^{-1}). The total silver was analyzed with an AAS (Perkin-Elmer Analyst 700 AAS, USA). Tetrazolium salt (MTT) bioassays were conducted to assess the inhibition ratio of the Ag clusters and citrate-stabilized AgNPs at different concentrations.[37–39] All of the experiments were performed in triplicate.

The MTT bioassay determined the ability of viable cells to reduce the yellow tetrazolium salt [3-(4,5-dimethylthiazol-2-yl)-2,5-diphenyltetrazolium bromide] (MTT) to blue formazan crystals by mitochondrial enzymes. The concentration of formazan crystals was spectrophotometrically determined when dissolved in acid-isopropanol. A volume of 0.2 mL of the thawed stock MTT solution was added to each vial at different inhibition periods, and vials were incubated under ambient conditions for 24 h. Acid-isopropanol (2 mL of 0.04 M HCl in isopropanol) was added to all of the vials and mixed thoroughly to dissolve the dark blue crystals. After incubation for 10 min at room temperature to ensure that all of the crystals were dissolved, the absorbance was measured at a wavelength of 570 nm using a UV-vis spectrophotometer. All of the samples were analyzed in triplicate.

3. Results and discussion

3.1. Synthesis mechanism and characterization

BSA was chosen as a reducing and capping agent in this study due to its merits in metal nanocluster synthesis. The silver complex $[Ag(S_2O_3)_2]^{3-}$ was required in this synthesis to avoid the precipitation of Ag^+ under alkaline conditions (Scheme 1). $[Ag(S_2O_3)_2]^{3-}$ was obtained by slowly dropping $AgNO_3$ into a $Na_2S_2O_3$ solution, and the moles of $AgNO_3$ used were less than those of $Na_2S_2O_3$. To ensure maximum contact with the silver complex, BSA was not denatured in case too many negative charges (groups such as –OH, $–NH_2$, and –COOH inside the protein scaffolds) will result in rejection with $[Ag(S_2O_3)_2]^{3-}$. The BSA reduced the silver complex to Ag^0 and stabilized the clusters in the solution.[33,34]

We demonstrate that BSA can reduce Ag^+ to Ag^0 and provide stability for the Ag nanoclusters during the formation process. Fig. S2 (ESI†) indicates the Ag^0 formation after incubation. The peaks of the Ag $3d_{5/2}$ binding energy appeared at 368.1 eV, which is consistent with the values ranging from 367.8 to 368.4 eV reported in previous studies.[40,41] To prepare AgNCs, freshly prepared $AgNO_3$ was slowly dropped into a $Na_2S_2O_3$ solution to form the silver complex $[Ag(S_2O_3)_2]^{3-}$ (eqn (1)). The moles of $AgNO_3$ were less than that of $Na_2S_2O_3$ to avoid the generation of a precipitate. Eqn (2) and (3) showed that a precipitate may be produced with higher amounts of $Na_2S_2O_3$. The silver complex is stable compared with Ag^+ in alkaline solution. As shown in Fig. S3 (ESI†), after reaction for 48 h, the initially colorless solution turned yellow at different pH values. An increase in the pH value gradually deepened the color of the Ag cluster solution. This trend corresponds to the UV-vis spectra recorded (Fig. S4A, ESI†). The peak is at 395 nm, which is a little shorter compared with the characteristic surface plasmon band of large Ag nanoparticles. The shorter wavelength corresponds to the smaller size of the nanoclusters.[32] The results indicate that Ag^+ had been reduced to Ag^0 after 48 h and that the amounts of silver nanoclusters increased with an increase in the pH value.

$$2Na_2S_2O_3 + AgNO_3 \rightarrow Na_3[Ag(S_2O_3)_2] + NaNO_3 \quad (1)$$

$$Na_2S_2O_3 + 2AgNO_3 \rightarrow Ag_2S_2O_3\downarrow + Na_2NO_3 \quad (2)$$

$$Ag_2S_2O_3 + 2H_2O \rightarrow Ag_2S\downarrow + S\downarrow + 2H_2SO_4 \quad (3)$$

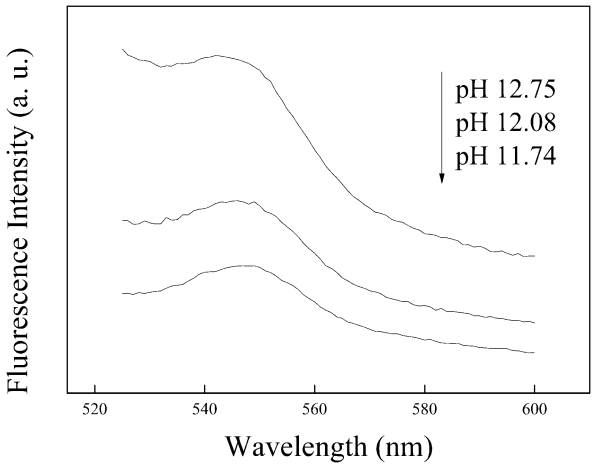

Fig. 1 Fluorescence emission spectra of prepared AgNCs illustrating the effect of pH during the synthesis of AgNCs. The initial BSA concentration was 0.88 g L^{-1}.

Fig. 1 exhibits the fluorescence spectra of the as-prepared AgNCs under the excitation of a 462 nm laser diode. The pH values were proven to play an essential role in the fluorescence intensity of our Ag clusters. An increase in the pH (Fig. 1) led to a gradual increase in the fluorescence intensity. When the pH was changed, we observed no obvious shift in the emission maximum at 548 nm. The emission peak indicated that the as-synthesized Ag clusters were green-emitting. The quantum yields of the formed Ag clusters were counted to be Φ = 0.23 in H_2O.

An increase in the pH led to a gradual decrease in the size (Fig. 2). This pH-dependent effect on the size was attributed to the stronger reducing capacity of thiol groups under higher alkaline conditions. The stronger reducing capacity resulted in formation of large numbers of small crystal nucleus, but not the larger one. More importantly, we observed an interesting phenomenon: the emission of the Ag clusters did not depend on their size. As shown in Fig. 2 compared with Fig. 1, three samples of Ag clusters with different sizes exhibited similar green spectra with an identical peak position; the only difference was the increase in the PL intensity with a decrease in the particle size. Fig. 2a–c indicate that the monodisperse Ag clusters

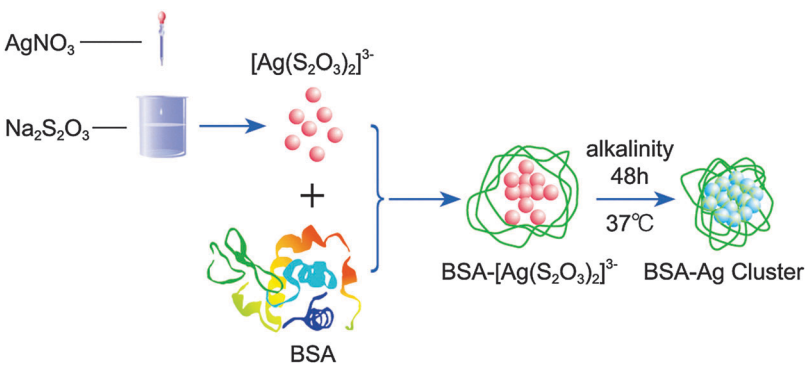

Scheme 1 Schematic of the BSA-directed synthesis of fluorescent AgNCs.

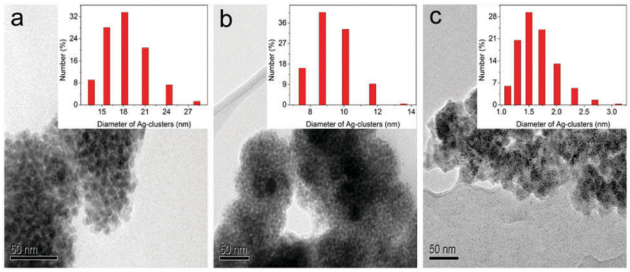

Fig. 2 TEM images of the as-prepared AgNCs synthesized at different pH values: (a) 11.74, (b) 12.08, and (c) 12.75. The inset shows the corresponding DLS histogram of the prepared clusters.

exhibit a narrow size distribution with average sizes of 18.1, 10.1, and 1.7 nm.

To investigate the structure and composition of the synthesized AgNCs, powder X-ray diffraction (XRD) and energy dispersive spectrometry (EDS) assays were employed. Fig. S4B (ESI†) shows the XRD pattern with peaks assigned to the corresponding diffraction signals of (111), (200), (220) and (311) facets of silver. The high intensity of the (111) peak indicates that the Ag clusters have a large number of (111) planes, thus making that peak the dominant reflection in the first diffraction feature. The EDS (Fig. S4C, ESI†) shows an obvious signal of Ag. The strong signals of C, O and S observed probably due to the presence of excess ligands at the surface of the clusters. Fig. S4D (ESI†) demonstrated that the clusters were stabilized by the –SH group containing BSA. The content of the –SH group at time 12 h was slightly decreased compared to that at 2 h, indicating the occurrence of reduction in the Ag cluster formation.

3.2. Hg^{2+} sensing using Ag clusters

3.2.1. Principle for Hg^{2+} detection. Many nanomaterials have been successfully applied in sensors,[42–45] and Ag clusters attracted a lot of attention.[46] It is well-known that elemental mercury can spontaneously react with the AgNP surface to form Ag/Hg amalgam.[47,48] The Ag clusters were covered with the –SH group containing BSA (curve c in Fig. S4D, ESI,† 1429 was the characteristic stretching vibration of thiol). After addition of various Hg^{2+} to the BSA capped Ag clusters, Hg^{2+} was immediately reduced to elemental mercury by the –SH group on BSA. Because of the high affinity between Ag and Hg, the reduced Hg(0) is directly deposited onto the Ag surface through the formation of Ag/Hg amalgam, thereby inducing a fluorescence quenching of Ag clusters. Fig. 3 shows the fluorescence spectra of Ag cluster solutions. In the presence of 10 000.0 nM Hg^{2+}, the fluorescence intensity of as-prepared Ag clusters quenched almost completely. PDCA was added as a masking agent of interfering ions such as Cu^{2+}. It was demonstrated that PDCA has little effect on the fluorescence emission of Ag clusters and does not work on Hg^{2+}.

3.2.2. Optimization of the Hg^{2+} sensing. In this study, the sensing time and reacting temperature are crucial for the probe sensitivity. Although a longer reaction time may yield a more stable fluorescence signal, it is unnecessary if the system has reached equilibrium. To obtain the optimal reaction time, the

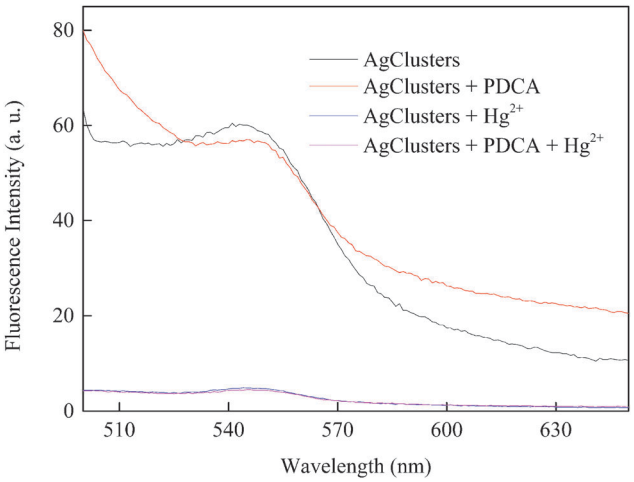

Fig. 3 Extinction spectra of Ag clusters.

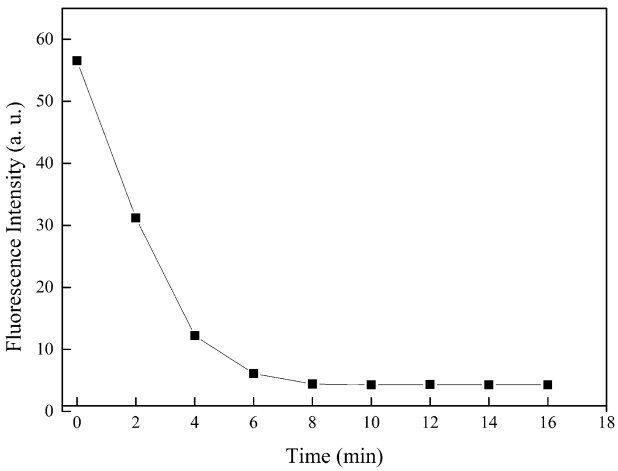

Fig. 4 Optimizing experiment of the sensing time. A value of 10 000.0 nM was selected as the Hg^{2+} concentration to determine the optimum reaction time. The fluorescence intensity was recorded at 548 nm.

kinetics of fluorescence quenching was measured. Fig. 4 showed the fluorescence intensity-reaction time curves of the Ag clusters after the addition of 10 000.0 nM Hg^{2+}. The fluorescence intensity was found to decrease with an increase in the reaction time, then reached a minimum at 8 min, and was nearly constant until 16 min. Based on these observations, we chose 9 min as the optimum reaction time to ensure completeness of the sensing process. To facilitate Hg^{2+} detection, the indoor temperature 25–27 °C was chosen as the operational temperature for all experiments. In view of the buffering ability of sodium phosphate buffer (the pH of buffer was 5.5–8.0), the experiments were carried out by adjusting the pH from 5.5 to 8.0. Fig. S5 (ESI†) showed the fluorescence extinction of the Ag clusters in reaction media at various pH values after the addition of 10 000.0 nM Hg^{2+}. The maximum quenching value in fluorescence was observed at pH 8.0 and then decreased with a decrease in pH values. Therefore pH 8.0 was chosen as the most suitable pH and was used in further experiments. All the experiments were conducted under these optimized conditions.

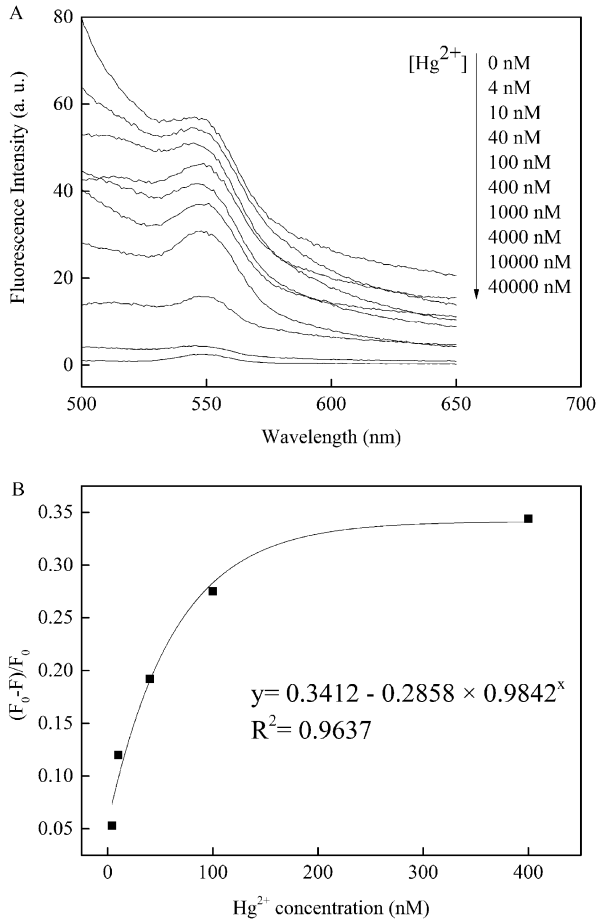

Fig. 5 (A) Extinction spectra of the working solutions containing Ag clusters after adding various concentrations of Hg^{2+} (0–40.0 μM) in buffer. (B) Exponential relationship between the fluorescence quenching and Hg^{2+} concentration in buffer. The concentrations of Hg^{2+} were 4.0, 10.0, 40.0, 100.0, and 400.0 nM. The fluorescence intensity was recorded at 548 nm.

3.2.3. Sensitivity for Hg^{2+}. Fig. 5A exhibits the fluorescence extinction spectra of Ag clusters after the addition of various concentrations of Hg^{2+}. The fluorescence intensity decreased gradually with an increase in Hg^{2+} concentration. It was obvious that, even at the lowest concentration of 4 nM, the fluorescence intensity exhibited a distinct change, which indicated that the proposed probe was sensitive enough for Hg^{2+} detection. Fig. 5B showed the exponential relationship between the fluorescence quenching rate at 548 nm and Hg^{2+} concentration (4.0–400.0 nM) in buffer. The fluorescence quenching rate was found to show an exponential dependence on the concentration of Hg^{2+} with the equation of $y = 0.3412 - 0.2858 \times 0.9842^{x}$ (where x is the concentration of Hg^{2+}, and y is the fluorescence quenching rate). The correlation coefficient was found to be 0.9643. When higher Hg^{2+} concentrations (1000.0, 4000.0, 10 000.0 and 40 000.0 nM) were taken into account, the relationship also showed good relevancy with a correlation coefficient of 0.9553 as shown in Fig. 6. The lowest detectable Hg^{2+} concentration was 4 nM, which meets the limit of detection requirements of Hg^{2+} in drinking water set by the U.S. Environmental Protection

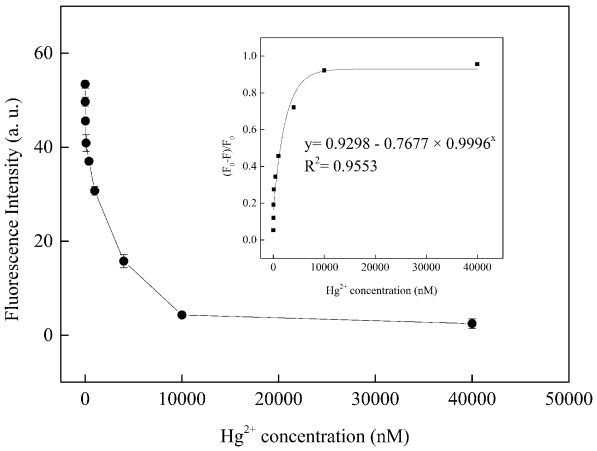

Fig. 6 The calibration curve of fluorescence intensity against Hg^{2+} concentration in buffer samples. Inset shows the response exponential relationship of the assay with Hg^{2+} concentrations at 4.0, 10.0, 40.0, 100.0, 400.0, 1000.0, 4000.0, 10 000.0 and 40 000.0 nM. The fluorescence intensity was recorded at 548 nm.

Agency (EPA).[49] In the previous study of Wang *et al.*,[50] the lowest detection limit of Hg^{2+} using BSA-capped Ag clusters was 25 nM. 3,3′,5,5′-Tetramethylbenzidine was needed to be oxidized in the detection process. In the work of Guo *et al.*,[3] although 10 nM can be obtained, an ice-bath was needed to accomplish BSA denaturation and centrifugation was required to remove excess saline that is produced in the denaturation process. Therefore, this method exhibits higher sensitivity compared to other BSA-capped Ag clusters in Hg^{2+} sensing, and the detection process is relatively convenient.[44]

3.2.4. Selectivity for Hg^{2+}. Fig. 7 exhibited the fluorescence quenching rate in the presence of various metal ions and mixed ions. The concentration of Hg^{2+} was 10.0 μM and 1.0 mM for each other ion. In contrast with the significantly greater

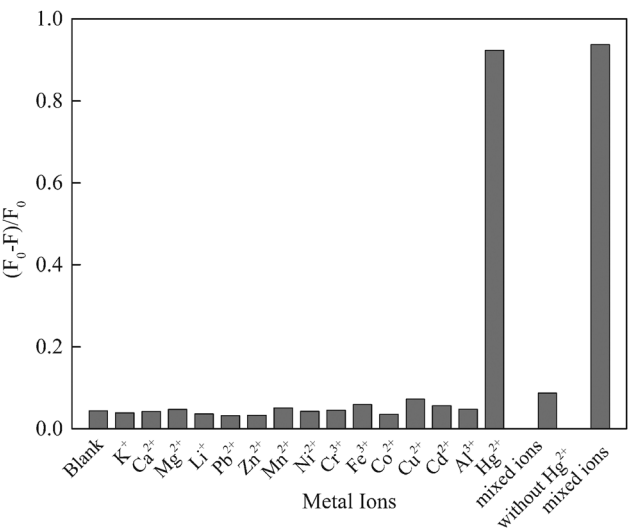

Fig. 7 Fluorescence quenching in the presence of various metal ions. The concentration is 1.0 mM for each metal ion and 10.0 μM for Hg^{2+}. The fluorescence intensity was recorded at 548 nm.

Table 1 Determination of Hg^{2+} (nM) in water samples using the proposed method and AFS

Sample	Added	Proposed method mean[a] ± SD[b]	AFS mean ± SD
Tap water 1	10.0	11.43 ± 0.11	10.12 ± 0.05
Tap water 2	50.0	51.79 ± 0.15	50.15 ± 0.13
Lake water 1	10.0	9.14 ± 0.14	9.21 ± 0.07
Lake water 2	50.0	49.67 ± 0.26	50.20 ± 0.08
River water 1	10.0	10.12 ± 0.10	10.24 ± 0.06
River water 2	50.0	51.66 ± 0.23	50.19 ± 0.10

[a] Mean of three determinations. [b] SD, standard deviation.

fluorescence quenching observed for Hg^{2+}, far weaker changes were observed upon the addition of mM concentrations of the other tested metal ions, revealing that this probe is selective for Hg^{2+}. As shown in Fig. 7, Cu^{2+} has a relatively lager fluorescence quenching rate than other metal ions except for Hg^{2+}. However, the fluorescence quenching rate was considerably low caused by Cu^{2+} when compared to that resulting from Hg^{2+} even though the concentration of Cu^{2+} was 100-fold higher than the concentration of Hg^{2+}. In addition, although the addition of the mixed metal ions without Hg^{2+} resulted in a slightly higher fluorescence quenching than that observed for the individual metal ions, the quenching rate was far greater in the presence of Hg^{2+}. These results indicated that the probe is sufficiently sensitive towards Hg^{2+} even in the environment containing several interfering ions.

3.2.5. Assays for real samples. To assess the practical application of the sensor in Hg^{2+} sensing, tap water, lake water and river water samples were employed in the detection process. For lake water and river water experiments, the samples collected were first filtered by qualitative filter paper and then centrifuged for 15 min at 10 000 rpm to remove oils and microbe impurities. The three samples were also boiled to remove the possible chlorine. The background concentration of mercury in the water samples was measured to be less than 0.1 nM using an atomic fluorescence spectrometer (AFS). All the samples were spiked with Hg^{2+} and measured by our proposed method and AFS. As shown in Table 1, the results measured by our proposed methods were in agreement with the value derived from AFS measurements. The results indicated high consistency in the determination of Hg^{2+} concentrations in environmental water samples by the proposed method with conventional instrumentation, demonstrating the excellent performance of this probe in practical applications.

3.3. Toxicity assays

It was demonstrated that the release of Ag ions from Ag nanomaterials and the production of ROS caused biotoxicity.[51–53] To quantify the respective contributions of the citrate-stabilized AgNPs *versus* the as-synthesized Ag clusters, the AgNPs and Ag clusters (Fig. S6 and S7, ESI†) were filtered, and their inhibition patterns at concentrations of 0.3, 0.5, and 1.0 μg mL^{-1} (Fig. 8) were compared at different times using the model species *Escherichia coli* (CMCC 44102). The maximum doses of the prepared citrate–AgNPs and BSA–Ag clusters, both of which are 1.0 mg mL^{-1}, resulted in 97.6% and 44.1% mortality, respectively, within the possible inevitable error (Fig. 8). This evident difference exhibits the excellent biocompatibility of the

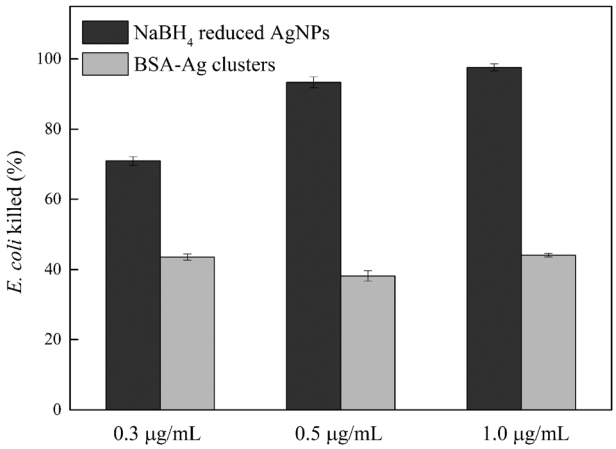

Fig. 8 Toxicity of BSA–Ag clusters compared with that of $NaBH_4$ reduced AgNPs.

BSA-synthesized Ag clusters. The higher bioavailability of the BSA–Ag clusters compared with the citrate–AgNPs may be explained by the lower toxicity of BSA. Furthermore, as the Ag clusters are formed, they become entrapped inside the protein. The functional groups inside the protein scaffolds, such as –OH, $–NH_2$, –COOH, and –SH, allow the clusters to more easily bind to cells. These entrapped clusters become stabilized by releasing Ag^+ to the environment due to the bulky nature of BSA.[27,28,35,36] As shown in Fig. 8, an increase in concentration resulted in a corresponding increase in the mortality to a certain extent. However, most of the inhibitory effects were no longer observed after 10 h. This time effect may contribute to the specific applications of these Ag clusters.

4. Conclusions

A convenient method for the synthesis of stable, water-soluble, green-emitting fluorescent Ag clusters was demonstrated using bovine serum albumin as a reducing and stabilizing agent. Bovine serum albumin reduces Ag^+ to Ag clusters and anchors the clusters through functional groups. Different Ag clusters of different sizes and fluorescent intensities were synthesized by controlling the alkaline conditions. The as-synthesized clusters are successfully applied in aqueous Hg^{2+} recognition and quantification with the lowest detectable concentration of 4.0 nM at a large range from 4.0 nM to 400.0 nM. These highly fluorescent Ag nanoclusters were more biocompatible than $NaBH_4$-reduced Ag nanoparticles. The protein capping may also avail numerous functional groups, which would result in the formation of clusters with potential applications in cell imaging and chemical and biosensing. In addition, one may expect that this biomimetic approach can be extended to the synthesis of other metal nanoclusters.

Acknowledgements

This study was financially supported by the National Natural Science Foundation of China (51579099, 51178171, 51521006,

51179068 and 51108166), the Program for Changjiang Scholars and Innovative Research Team in University (IRT-13R17).

Notes and references

1 J. Zheng, P. R. Nicovich and R. M. Dickson, *Annu. Rev. Phys. Chem.*, 2007, **58**, 409–431.
2 Y. Y. Cui, Y. Y. Wang, R. Liu, Z. P. Sun, Y. T. Wei, Y. L. Zhao and X. Y. Gao, *ACS Nano*, 2011, **11**, 8684–8689.
3 C. Guo and J. Irudayaraj, *Anal. Chem.*, 2011, **83**, 2883–2889.
4 R. L. Whetten, J. T. Khoury, M. M. Alvarez, S. Murthy, I. Vezmar, Z. L. Wang, P. W. Stephens, C. L. Cleveland, W. D. Luedtke and U. Landman, *Adv. Mater.*, 1996, **8**, 428–433.
5 R. L. Whetten, M. N. Shafigullin, J. T. Khoury, T. G. Schaaff, I. Vezmar, M. M. Alvarez and A. Wilkinson, *Acc. Chem. Res.*, 1999, **32**, 397–406.
6 A. C. Templeton, M. P. Wuelfing and R. W. Murray, *Acc. Chem. Res.*, 2000, **33**, 27–36.
7 H. X. Xu and K. S. Suslick, *Adv. Mater.*, 2010, **22**, 1078–1082.
8 J. P. Wilcoxon and B. L. Abrams, *Chem. Soc. Rev.*, 2006, **35**, 1162–1194.
9 J. A. Alonso, *Chem. Rev.*, 2000, **100**, 637–678.
10 Y. Wang, J. Chen and J. Irudayaraj, *ACS Nano*, 2011, **5**, 9718–9725.
11 J. T. Petty, D. A. Nicholson, O. O. Sergev and S. K. Graham, *Anal. Chem.*, 2014, **86**, 9220–9228.
12 L. Zhang, J. Zhu, Z. Zhou, S. Guo, J. Li, S. Dong and E. Wang, *Chem. Sci.*, 2013, **4**, 4004–4010.
13 R. C. Jin, *Nanoscale*, 2010, **2**, 343–362.
14 F. Qu, N. B. Li and H. Q. Luo, *Anal. Chem.*, 2012, **84**, 10373–10379.
15 I. Rabin, W. Schulze and G. Ertl, *Chem. Phys. Lett.*, 1999, **312**, 394–398.
16 N. Cathcart, P. Mistry, C. Makra, B. Pietrobon, N. Coombs, M. Jelokhani-Niaraki and V. Kitaev, *Langmuir*, 2009, **25**, 5840–5846.
17 B. Adhikari and A. Banerjee, *Chem. Mater.*, 2010, **22**, 4364–4371.
18 H. Xu and K. S. Suslick, *ACS Nano*, 2010, **4**, 3209–3214.
19 W. Guo, J. Yuan, Q. Dong and E. Wang, *J. Am. Chem. Soc.*, 2010, **132**, 932–934.
20 T. Vosch, Y. Antoku, J. C. Hsiang, C. I. Richards, J. I. Gonzalez and R. M. Dickson, *Proc. Natl. Acad. Sci. U. S. A.*, 2007, **104**, 12616–12621.
21 H. C. Yeh, J. Sharma, J. J. Han, J. S. Martinez and J. H. Werner, *Nano Lett.*, 2010, **10**, 3106–3110.
22 J. T. Petty, C. Fan, S. P. Story, B. Sengupta, A. St. John Iyer, Z. Prudowsky and R. M. Dickson, *J. Phys. Chem. Lett.*, 2010, **1**, 2524–2529.
23 J. T. Petty, J. Zheng, V. Nicholas and R. M. Dickson, *J. Am. Chem. Soc.*, 2004, **126**, 5207–5212.
24 C. I. Richards, S. Choi, J. C. Hsiang, Y. Antoku, T. Vosch, A. Bongiorno, Y. L. Tzeng and R. M. Dickson, *J. Am. Chem. Soc.*, 2008, **130**, 5038–5039.
25 X. L. Guevel, B. Hötzer, G. Jung, K. Hollemeyer, V. Trouillet and M. Schneider, *J. Phys. Chem. C*, 2011, **115**, 10955–10963.
26 J. Xie, Y. Zheng and J. Y. Ying, *J. Am. Chem. Soc.*, 2009, **131**, 888–889.
27 A. Mathew, P. R. Sajanlal and T. Pradeep, *J. Mater. Chem.*, 2011, **21**, 11205–11212.
28 I. Díez and R. H. A. Ras, in *Advanced Fluorescence Reporters in Chemistry and Biology II*, ed. A. P. Demchenko, Springer, Berlin, 2010, vol. 9, pp. 307–332.
29 T. U. B. Rao and T. Pradeep, *Angew. Chem., Int. Ed.*, 2010, **49**, 3925–3929.
30 J. P. Xie, Y. G. Zheng and J. Y. Ying, *Chem. Commun.*, 2010, **46**, 961–963.
31 S. J. Hurst, H. D. Hill and C. A. Mirkin, *J. Am. Chem. Soc.*, 2008, **130**, 12192–12200.
32 J. Yu, S. A. Patel and R. M. Dickson, *Angew. Chem., Int. Ed.*, 2007, **46**, 2028–2030.
33 J. Xie, J. Y. Lee, D. I. C. Wang and Y. P. Ting, *ACS Nano*, 2007, **1**, 429–439.
34 I. Diéz and H. A. Ras, *Nanoscale*, 2011, **3**, 1963–1970.
35 U. Anand, S. Ghosh and S. Mukherjee, *J. Phys. Chem. Lett.*, 2012, **3**, 3605–3609.
36 J. Y. Liu and R. H. Hurt, *Environ. Sci. Technol.*, 2010, **44**, 2169–2175.
37 Y. Liu and M. G. Nair, *J. Nat. Prod.*, 2010, **77**, 1193–1195.
38 Y. Cetin and L. B. Bullerman, *J. Agric. Food Chem.*, 2006, **54**, 1949–1955.
39 T. Mosmann, *J. Immunol. Methods*, 1983, **65**, 55–63.
40 H. Deng, Y. Yu, F. Liu, J. Ma, Y. Zhang and H. He, *ACS Catal.*, 2014, **4**, 2776–2784.
41 H. He, Y. Li, X. Zhang, Y. Yu and C. Zhang, *Appl. Catal., A*, 2010, **375**, 258–264.
42 H. Wei, Z. Wang, L. Yang, S. Tian, C. Hou and Y. Lu, *Analyst*, 2010, **135**, 1406–1410.
43 T. Chen, Y. Hu, Y. Cen, X. Chu and Y. Lu, *J. Am. Chem. Soc.*, 2013, **135**, 11595–11602.
44 J. Duan and J. Zhan, *Sci. China Mater.*, 2015, **58**, 223–240.
45 Y. Hu, W. Guo and H. Wei, *Isr. J. Chem.*, 2015, **55**, 682–697.
46 Y. Ding, L. Shi and H. Wei, *J. Mater. Chem. B*, 2014, **2**, 8268–8291.
47 L. Deng, X. Y. Ouyang, J. Y. Jin, C. Ma, Y. Jiang, J. Zheng, J. S. Li, Y. H. Li, W. H. Tan and R. H. Yang, *Anal. Chem.*, 2013, **85**, 8594–8600.
48 Z. Guo, G. Chen, G. Zeng, Z. Li, A. Chen, M. Yan, L. Liu and D. Huang, *RSC Adv.*, 2014, **4**, 59275–59283.
49 http://water.epa.gov/drink/contaminants/basicinformation/mercury.cfm#four.
50 G. L. Wang, L. Y. Jin, X. M. Wu, Y. M. Dong and Z. J. Li, *Anal. Chim. Acta*, 2015, **871**, 1–8.
51 Z. M. Xiu, J. Ma and P. J. Alvarez, *Environ. Sci. Technol.*, 2011, **45**, 9003–9008.
52 E. Navarro, A. Baun, R. Behra, N. B. Hartmann, J. Filser, A. J. Miao, A. Quigg, P. H. Santschi and L. Sigg, *Ecotoxicology*, 2008, **17**, 372–386.
53 Z. Wang, T. Xia and S. Liu, *Nanoscale*, 2015, **7**, 7470–7481.